

Saccade crossing avoidance as a visual search strategy

Alex Szorkovszky^{1,*}, Rujeena Mathema^{2,3}, Pedro Lencastre^{2,3}, Pedro Lind^{1,2,3,4}, and Anis Yazidi^{2,3,5}

¹Department of Numerical Analysis and Scientific Computing, Simula Research Laboratory, Oslo, Norway

²Department of Computer Science, Oslo Metropolitan University, Oslo, Norway

³OsloMet Artificial Intelligence Lab, Oslo Metropolitan University, Oslo, Norway

⁴School of Economics, Innovation and Technology, Kristiania University of Applied Sciences, Oslo, Norway

⁵Department of Informatics, University of Oslo, Oslo, Norway

*E-mail: alex@simula.no

Abstract

Although visual search appears largely random, several oculomotor biases exist such that the likelihoods of saccade directions and lengths depend on the previous scan path. Compared to the most recent fixations, the impact of the longer path history is more difficult to quantify. Using the step-selection framework commonly used in movement ecology, and analyzing data from 45-second viewings of *Where's Waldo?*, we report a new memory-dependent effect that also varies significantly between individuals, which we term self-crossing avoidance. This is a tendency for saccades to avoid crossing those earlier in the scan path, and is most evident when both have small amplitudes. We show this by comparing real data to synthetic data generated from a memoryless approximation of the spatial statistics (i.e. a Markovian nonparametric model with a matching distribution of saccade lengths over time). Maximum likelihood fitting indicates that this effect is strongest when including the last ≈ 7 seconds of a scan path. The effect size is comparable to well-known forms of history dependence such as inhibition of return. A parametric probabilistic model including a self-crossing penalty term was able to reproduce joint statistics of saccade lengths and self-crossings. We also quantified individual strategic differences, and their consistency over the six images viewed per participant, using mixed-effect regressions. Participants with a higher tendency to avoid crossings displayed smaller saccade lengths and shorter fixation durations on average, but did not display more horizontal, vertical, forward or reverse saccades. Together, these results indicate that the avoidance of crossings is a local orienting strategy that facilitates and complements inhibition of return, and hence exploration of visual scenes.

Statistically speaking, visual scan paths when viewing scenes look remarkably like random walks, particularly when salient areas are evenly distributed [1, 2]. Comparisons have frequently been made to animal foraging [3] — although in the case of vision, movement occurs primarily in discrete steps (saccades), between which are relatively still periods (fixations). Yet, as with animal foraging, there are task-dependent biases and patterns that can be uncovered if enough eye-tracking data is recorded [4].

Some biases, such as a tendency for the eyes to relax towards the centre of vision, can be specified as a simple function of the most recent fixation (i.e. fixations from this point toward the centre become more likely than in the opposite direction). In general, a Markovian model such as $P(x_{t+1}, y_{t+1} | x_t, y_t)$ [5], when combined with saliency modelling, can come close to deep learning models in predicting the next fixation [6]. Such a distribution is also low-dimensional enough to generate with nonparametric methods [7].

Other biases depend on the most recent saccade (i.e. the two most recent fixations), such as the increased likelihood of forward and return saccades, which continue with the same length and in the same or reverse

direction, respectively [8]. In other directions, regular changes in saccade length are more common than what is expected if subsequent lengths are assumed to be independent, leading to a negative autocorrelation [9].

Finally, some biases have longer history-dependence. The probability of saccades returning to ‘ k -back’ fixations decreases only slowly with k in some tasks [8]. This is has been called “facilitation of return” [10], in competition with “inhibition of return” which supposedly facilitates exploration [11]. It has been proposed that the former bias applies for salient points which require further consideration [8], while the latter is more prominent for simple distractors and low working memory demands [12].

The aforementioned influences on saccade dynamics have been quantified and modelled in various ways. Often they are based on comparing distributions of saccade and fixation measures to models assuming the absence and/or presence of some effect. The distributions compared (such as saccade length or change in saccade angles) depends on the phenomenon being examined. While there have been recent attempts to unify modeling approaches under the banner of likelihood-based inference [13], this has mainly been applied to comparing overall models against a benchmark rather than comparing the importance of predictors within models.

Another difficulty with identifying history dependence is the short length of most tasks and datasets. Deep learning models have been used to show that up to four fixations can increase predictive power in free viewing [14]. However, given what is known about refixations, it is expected that humans should be able to keep track of a longer scan path during search.

Here, we use step selection analysis, a case-control sampling based method common in studies of animal movement [15], to quantify biases and long-term history dependence in scan paths during visual search. There are several advantages of this approach: Firstly, by using a typical saccade model to sample both taken and available steps, it can account for the fact that no two data points will have the same path history (in analogy with the heterogeneity of environmental features encountered by animals as they move). Secondly, being compatible with general regression models, it can evaluate the relative importance of and interactions between known biases in a straightforward way. Thirdly, by including random effects, it can also capture repeatable variation in biases between individuals [16], which would otherwise require a large amount of data per individual to quantify. Previous studies of strategic variation have focused on simple measures such as saccade frequency [17]. Given that visual search performance is correlated with several personality traits and cognitive abilities [18], we expect the underlying strategy to vary consistently along several other measures. While consistent differences have been identified in saccade lengths and fixation durations across tasks and time [19, 20, 21], stable patterns involving several measures have not yet been identified in visual search.

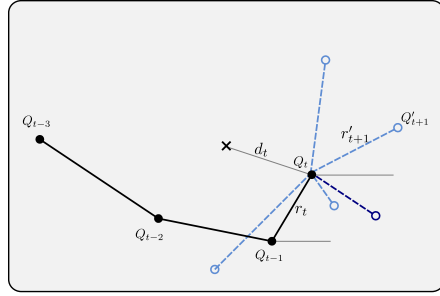
In addition to the most commonly reported biases and memory-dependent effects, we propose a new bias that we term *self-crossing avoidance*. This is inspired by the concept of space-filling curves, which exhibit this feature as a means to efficiently cover an area. The concept of self-avoiding random walks has also been explored by Engbert et al. to explain the statistics of small-scale eye movements during fixations [22], although in this case self-avoidance emerges from a combination of inhibition and a uniform microsaccade length. Instead, we include the number of recent saccades that are crossed by a candidate saccade as a potential influence on its likelihood.

We use the book series *Where’s Waldo*, which has been used for several other studies of visual search [11, 23, 24, 25]. With a high density of salient and heterogeneous distractors, this is a relatively difficult search task compared to natural scenes [25] and categorical target-distractor paradigms [26]. It is known that the density of visual features influence search patterns [26]. However, the relative homogeneity of the Waldo paradigm presents a task where the search space is not biased by more and less salient regions. Therefore, this is highly suitable for “pure” image-independent scan-path modelling, as well as for uncovering variation in search strategies.

To compare the search task to a bottom-up free viewing, we also use stimuli consisting of random coloured pixels, in which the participant is instructed to look for shapes and patterns hidden in the image. This presents another homogeneous stimulus favourable to identifying differences between individual scan patterns [27].

a

Predictor	Definition	L_{hist}
Log length	$\log(r'_{t+1,t})$	1
Cardinality	$\cos(4\phi'_{t+1})$	1
Horizontal bias	$\cos(2\phi'_{t+1})$	1
Centre dist change	$d'_{t+1} - d_t$	1
Parallel bias	$\cos(2\phi'_{t+1} - 2\phi_t)$	2
Forward bias	$\cos(\phi'_{t+1} - \phi_t)$	2
Length change	$ \log(r'_{t+1,t}/r_{t,t-1}) $	2
1-back distance	$r'_{t+1,t-1}$	2
Visited point	$I\left[\sum_{i:T_i > T_1 - \tau_1} I(r'_{t+1,i} < r_0) > 0\right]$	any
Sparsity ν'_{t+1}	$\mathbb{E}_{i:T_i > T_1 - \tau_2} [r'_{t+1,i}] / \sup_{i:T_i > T_1 - \tau_2} (r'_{t+1,i})$	any
Sparsity change	$\nu'_{t+1} - \nu_t$	any
Crossings	$\sum_{i:T_i > T_1 - \tau_3} I(Q_i Q'_{t+1} \cap Q_{i-1} Q_i \neq \emptyset)$	any



b

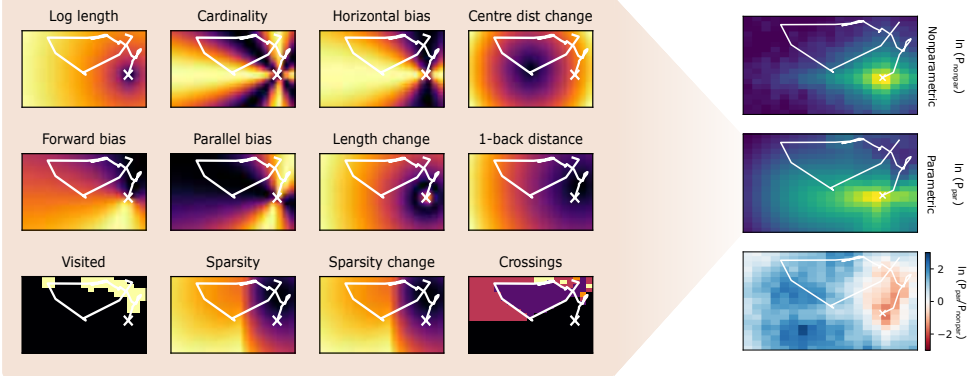


Figure 1: (a) List of predictors used (left), and an example of a scan path illustrating key quantities and case-control sampling (right). Predictors are sorted by the number of most recent fixations L_{hist} required to calculate them. In the illustration, predictors are calculated for fixation Q_{t+1} by generating four random control saccades (light dotted lines) in addition to the saccade from the data (dark dotted line). The center of the screen is indicated by a cross. (b) The panels on the left illustrate parametric predictor values for test points Q'_{t+1} given a scan path up to Q_t indicated by a cross. The panels on the right show overall spatial log likelihoods for the nonparametric model (top) the combined parametric model (middle) and the difference (bottom).

Results

The predictors used are defined in Figure 1 and visualized for a sample scan path. The predictors that depend on more than one previous saccade each contain a time constant that truncates the history length. These were optimized first separately and then jointly to maximize the likelihood of the logistic regression model (see Supplementary Information). For the Waldo task, the binary *visited point* predictor, indicating whether or not the candidate point was within 1.5 degrees (approximately the foveal angle) of a recent fixation, was optimal at $\tau_1 = 6$ s. The *sparsity* predictor, quantifying the ratio of the mean to maximum distance of previously visited points, was strongest when τ_2 was set to 32 seconds. Finally, the *self-crossing* predictor, indicating the number of times a candidate saccade crossed the recent scan path, was optimal at $\tau_3 = 7$ seconds. When optimized jointly, τ_1 , τ_2 and τ_3 moved to 4, 33 and 6 seconds respectively. The three features therefore appear to capture complementary aspects of the path dependence, as shown by the lack of strong dependence between the time constants (see Supplementary Figure S1).

The sparsity measure, along with the distance from the center, partially capture how fixations were distributed overall within the screen area and among previous fixations. As shown in Figure 2(a-b), these

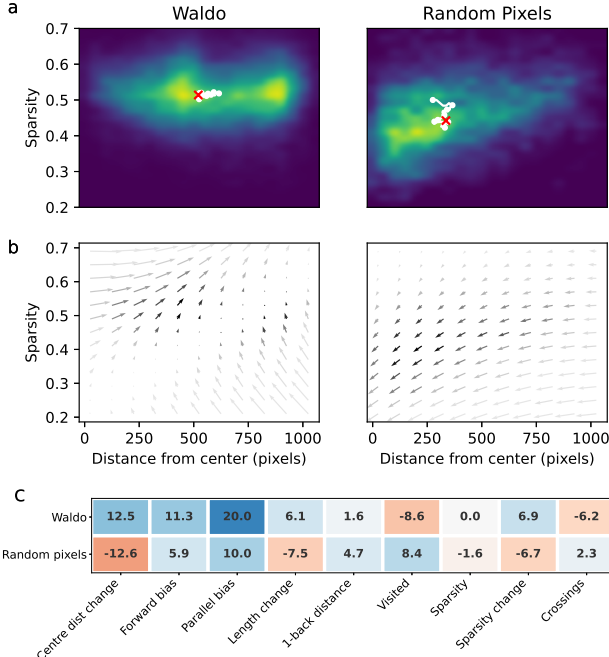


Figure 2: Task comparison. The panels in (a) compare the spatial distributions of fixations in terms of sparsity and distance from the centre of the image. Overlaid are moving averages over time, with a window length of 5 seconds, ending in the red crosses. The arrows in (b) shows the direction and slope of maximum gradient in log-odds from fitted parametric models evaluated at the small-saccade limit $Q'_{t+1} \approx Q_t$ (see Supplementary Information). Panel (c) compares normalized z-scores for the main predictors in the model. The color of each cell gives the normalized z-score when including only a linear term for this predictor and all interactions for all other terms. Terms that do not decrease the AIC are given a normalized z-score of zero. Log-length, horizontal bias and cardinality are not included due to strong dependence on the saccade model.

distributions differ strongly between the the two tasks. Panel (b) shows that for the Waldo task, the likelihood of shifts in these quantities were more dependent on their current values; while (c) shows that, overall, changes in these predictors had opposite effects on fixation likelihood.

As expected, the history-independent predictors were the strongest overall, as shown in Figure 2(c) and Supplementary Figure S4. *Parallel bias*, which equally captures forward and return saccades, was the strongest linear predictor in the Waldo dataset. This and the additional *forward bias* were the only predictors that were in the same direction for the random pixel data. The predictors related to previously visited points indicated an inhibition of return on average in the Waldo task, as shown by the positive effect of change in sparsity and negative effect of a candidate fixation being close to one in its recent history, and conversely a facilitation of return for the random pixel task.

For the Waldo task, synthetic data was generated to further investigate the self-crossing statistics. A nonparametric and memoryless null model was fit, based on a kernel-smoothed empirical distribution $P(\Delta x_t, \Delta y_t | x_t, y_t)$. To control for the well-known coarse-to-fine transition [28], in which mean saccade length decreases over time, a cubic spline was fit to the saccade log-length as a function of time. Generated saccades were then rescaled according to this curve. The resulting generative model matched the overall distribution of saccade lengths for the entire trial length (see Figure 3(a) and Supplementary Figure S3). For comparison, the same amount of data was also generated using the parametric model fit by the step selection process.

For disconnected and independent line segments, crossing probability is expected to increase proportion-

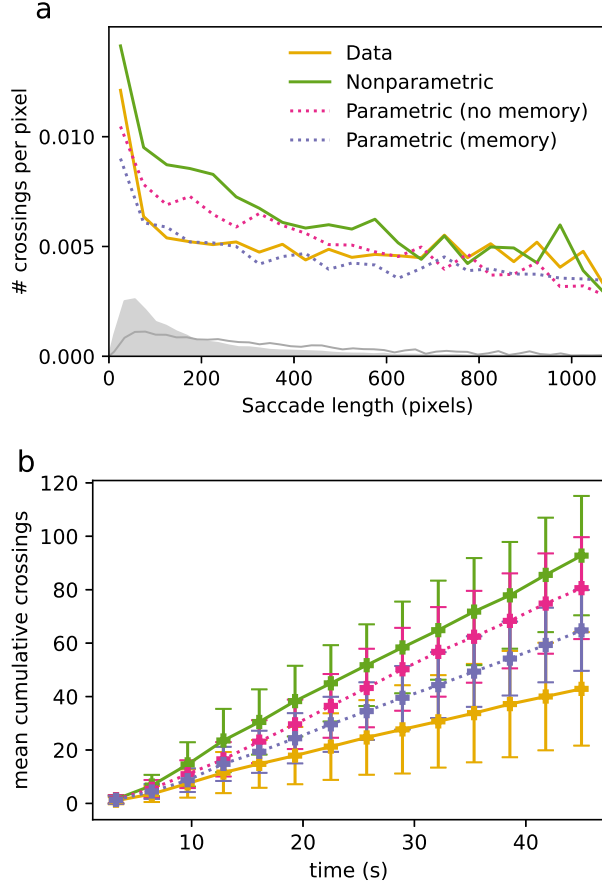


Figure 3: (a) Mean number of crossings (including intersections with both past and future saccades within τ_3) divided by saccade length, plotted against saccade length, for the models and test data. The grey area shows the density of saccade lengths in the test data, while the grey line shows the density of saccades with crossings. (b) Cumulative number of crossings over time for data generated from each model along with the test data. Shown are means and standard deviations over all 70 trials in each set.

ally to length [29]. Here, since fixations are spatially clustered, there is a decreased probability of crossing per unit length for longer saccades (see Figure 3a). Compared to the null model, the experimental data showed relatively fewer crossings for all saccades, apart from the longest $\approx 15\%$ (above 350 pixels) and those within the foveal angle. The trend was closely matched by the memory-dependent parametric model. This was also true for “crossing” and “crossed” saccades separately (see Supplementary Figure S5), despite existing saccade lengths not being a model input.

Overall, the mean number of crossings per saccade was 0.59 compared to 0.33. As shown in Figure 3b, the full parametric model was closer to the crossing distribution of the data than of the null model, with a mean of 0.43 crossings per saccade.

Random effects were then added sequentially to each feature of a linear step selection model to quantify the individual variation in search strategies. For the Waldo task, all features had a significant participant effect (according to a lower AIC) apart from *center distance change*, *fixation sparsity* and *fixation sparsity change*. The intraclass-correlation coefficient, quantifying how much of the variation across trials was due to inter-participant variation, was highest for length change and self-crossing variance (ICC 0.91 and 0.80 respectively, see Figure 4(a)).

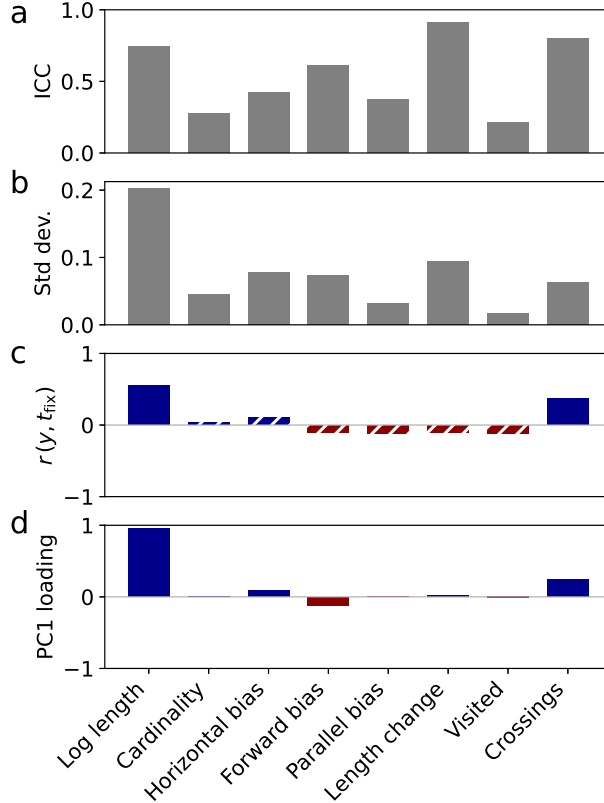


Figure 4: Waldo task individual differences. (a) Intraclass correlation coefficients for predictors where there was significant variation among both trials and participants. (b) Corresponding standard deviations of the participant-level random effect. (c) Pearson correlation coefficients between each significant random participant effect (y) and the mean of the trial-level median fixation duration t_{fix} . Hatched bars indicate lack of significance at the $p < 0.05$ level. (d) Loadings of the first principal component given the fitted means for each participant and each significant predictor.

Several predictors were also positively correlated with those fitted for the random pixel task (without trial effects in the latter models due to the low number of trials per participant) at the $p < 0.05$ level, with only *cardinality*, *length change* and *visited* predictors not being significant. The remaining correlations ranged from $r = 0.42$ for self-crossing avoidance to $r = 0.58$ for parallel bias.

The significant participant-level random effects for log length and self-crossings were positively correlated with average fixation durations in the same task (see Figure 4c, Supplementary Figure S8). When averaged over all participants, fixation time was greater for the random pixel task (mean 0.40 vs 0.27 for Waldo, t-test $t = 10.3, p = 10^{-11}$). Despite this large overall difference, the individual-level average fixation times were positively correlated between the two tasks (Pearson $r = 0.43, p = 0.016$).

When dimensionality of the unscaled random effects was reduced using principal component analysis, the first component captured 65% of the variance for the Waldo task. Participants that scored high on this component took longer steps, with more self-crossings (see Figure 4d). As was the case for these predictors on their own, the first principal component was also correlated with mean fixation duration ($r = 0.54, p = 0.002, n = 31$). The second principal component, with 19% variance explained, was highest for participants with more forward bias, more horizontal bias, and less alternation in saccade length (see Supplementary Figure S9). The PCA loadings for the random pixel task were markedly different, and were not correlated with fixation time. However, the random effects for change in centre distance and parallel

bias were negatively correlated with mean fixation time in this case (see Supplementary Figure S6).

Discussion

Difficult visual search tasks can take a considerable amount of time, providing ample opportunities to investigate participants' search strategies as well as cognitive and oculomotor biases. The latter are more often studied using short-length free-viewing datasets designed for studying saliency, since these are much more widely available [6]. This means that long-term effects are generally under-appreciated when studying scan paths.

Using the step selection framework allowed various influences on the scan path to be considered simultaneously and to be compared on an equal footing. This technique is therefore suitable for tasks such as free viewing or visual search of scenes, and lessens the need for exhaustive experimental manipulations which, while often cleverly designed [30], ultimately lessen ecological validity. Although we did not use image features, assuming approximately uniform salience, step selection also allows the integration of aspects of saliency for comparing top-down and bottom-up influences on the scan path.

As is well known, participants looking at random, information-poor images will tend to focus more on the center of the image [27]. We have shown that in addition to the image center, several other influences have not only different strengths when comparing search and free viewing, but the effects are in opposite directions.

Since the resolution of spatial information in memory decreases over time [31], the longest term predictors should be the ones that require the least spatial resolution. Consistent with this, our fixation sparsity measure is insensitive to small changes in the scan path history, while the visited point predictor requires a resolution at the level of the foveal area.

The self-crossing tendency showed strong inter-individual variation and, on average, indicated avoidance during search. Those who avoided crossings more strongly also tended to make shorter saccades. This could mean that some participants pursued a systematic strategy of organized scan paths, as shown in [32] for stimuli on a grid. However, this would also imply strong variation in and correlation with cardinality, which was not seen in our data. We found that crossing shorter saccades tended to be avoided compared to the null model. This is consistent with the shorter optimal history length for this predictor.

Another clue for the functional significance of this variation can be found in the duration of fixations, which was absent from the step selection modelling. Fixation durations, widely used as a proxy for focused visual processing, were correlated at the individual level with saccade length and self-crossings in the Waldo task, which comprise the primary axis of variation in this task. Unlike the commonly found negative relationship between saccade length and fixation duration, as seen when comparing ambient and focal viewing over time [33], or between novices and experts [34], this relationship was instead found to be positive at the inter-individual level for the Waldo task. Such a relationship at the inter-individual level has been reported for free viewing [35], but previous studies for search, such as Henderson and Luke [21], may have had too small a sample size to reach statistical significance. Resolution of this effect may have also been enhanced in our case by using log-transforms for saccade length, which typically has a long-tailed distribution.

We also found that participants that were more likely to avoid self-crossings used shorter fixations on average. This may indicate that self-crossing avoidance is used primarily during the faster process of spatial orientation [36], and some participants use more of this "ambient" processing. In aviation, for example, experts use more complex scan paths and shorter fixations than amateurs [37]. Together, this may indicate that avoiding crossing of recent saccades is a relatively simple orienting strategy that facilitates exploration and complements explicit inhibition of return to recently visited locations.

This work also has implications for deep learning scan path models. The state-of-the-art Deepgaze III model [14] uses three images per fixation to encode their positions, so that they can be input into a convolutional neural network (CNN) and combined with a saliency map. This means that the size of the scanpath network will be proportional to the desired history length. Therefore, for deep learning to be useful in modeling human attention during complex search, it may be necessary to find more compact

representations of history. Heatmaps of our three long time-scale heuristics, which we included for illustration, may also be useful as CNN inputs in this respect.

We have demonstrated a new and powerful method for quantifying oculomotor biases, leveraging techniques used in movement ecology. We expect that incorporating image features may provide both competitive and insightful results on common saliency benchmarks. Future work that correlates strategic variation with cognitive and personality differences may also shed light on the ways neural circuitry is recruited during visual search.

Materials and Methods

Data

31 participants, using chin rests approximately 1 meter from a 1920x1080 pixel monitor, were each shown nine *Where's Waldo* images that filled the screen for 45 seconds each, followed by three images comprised of randomized RGB values per pixel, for 60 seconds each. Eye gaze was tracked using the EyeLink Duo at 1000Hz frame rate. Saccades and fixations were automatically extracted using the software. One in every four trials were reserved as a test set, distributed evenly among individuals and among images, with the remaining used for training the generative models. All data was used for the final fitting of mixed effect models.

Step selection

Importance sampling was used for generating control points [38, 39]. For each real data point, nine control data points were generated from a radially symmetric lognormal distribution fitted to the training set, with sampling repeated for any points generated outside the image boundary. For each data point, all predictors were calculated, along with the square of the log-length. These were then fed into a logistic regression to separate data points from control points. All interaction terms were initially included, and stepwise selection was used to remove insignificant interaction terms (see Supplementary Information). An interaction term between log length and time was also included to capture the coarse-to-fine transition [28]. These regressions were done using the Python *statsmodels* package.

Time constant optimization

For each variable-history predictor, the cutoff τ was iterated in units of one second up to the trial length of 45 seconds (see Supplementary Information). The value of τ maximizing the likelihood of the step selection, when including this predictor, the short-term predictors and all interactions, was then obtained and used for the rest of the analysis. For fixation sparsity, both the sparsity and the change in sparsity were included with the same value of τ_2 .

Nonparametric generative model

Gaussian kernel density estimation was used to smooth the conditional empirical distribution of $P(\Delta x_i, \Delta y_i | x_i, y_i)$. One variance was used for x, y and another was used for Δ_x, Δ_y , and these were optimized jointly (see Supplementary Information). This was sampled from directly to generate synthetic data. To account for the change in average saccade length over time, a cubic spline was fit to the empirical log-length against time. Saccade lengths were then adjusted based on the time in the simulation according to the spline. Any points outside the boundary of the image were discarded and resampled. Time intervals between fixations were sampled from its unconditional distribution, which determined the total number of fixations within the trial length.

Parametric generative model

At each time step, 40 candidate points were generated as for the step selection process, resampling any outside the image boundary. The fitted step selection model was then used to estimate the likelihood of each point, adjusting the intercept term for the difference in number of samples. One sample was then chosen with a probability proportional to this likelihood. Time intervals were sampled from the unconditional distribution as for the nonparametric model.

Mixed-effect modelling

Individual variation was tested and quantified using a binomial mixed effect regression. All predictors were first centered and normalized. In the Waldo task, for each of the fixed effects, a term modeling the slope varying over trials (279, nine per participant, variance σ_t^2) was tested first against the base model with only fixed effects using the AIC. If the mixed model had a lower AIC, a second random slope effect was included for participant (31, variance σ_p^2), and also tested using the AIC. For predictors with a significant participant effect, the ratio $\sigma_p^2/(\sigma_p^2 + \sigma_t^2)$ was used as the intraclass correlation coefficient (ICC). For the random pixel task, only one test was performed for the participant effect, due to the small number of trials, and thus the ICC was not obtained. The *R* package *lme4* was used via the Python package *pymer4*[40].

Acknowledgements

This work is funded by the Research Council of Norway's FRIPRO grant number 335940.

References

- [1] Giuseppe Boccignone and Mario Ferraro. Modelling gaze shift as a constrained random walk. *Physica A: Statistical Mechanics and its Applications*, 331(1-2):207–218, 2004.
- [2] Heiko H Schütt, Lars OM Rothkegel, Hans A Trukenbrod, Sebastian Reich, Felix A Wichmann, and Ralf Engbert. Likelihood-based parameter estimation and comparison of dynamical cognitive models. *Psychological review*, 124(4):505, 2017.
- [3] Marcos Bella-Fernández, Manuel Suero Sune, and Beatriz Gil-Gómez de Liaño. Foraging behavior in visual search: A review of theoretical and mathematical models in humans and animals. *Psychological research*, 86(2):331–349, 2022.
- [4] Benjamin W Tatler and Benjamin T Vincent. The prominence of behavioural biases in eye guidance. *Visual Cognition*, 17(6-7):1029–1054, 2009.
- [5] Alasdair DF Clarke, Matthew J Stainer, Benjamin W Tatler, and Amelia R Hunt. The saccadic flow baseline: Accounting for image-independent biases in fixation behavior. *Journal of vision*, 17(11):12–12, 2017.
- [6] Matthias Kümmerer and Matthias Bethge. State-of-the-art in human scanpath prediction. *arXiv preprint arXiv:2102.12239*, 2021.
- [7] Pedro Lencastre, Marit Gjersdal, Leonardo Rydin Gorjão, Anis Yazidi, and Pedro G Lind. Modern ai versus century-old mathematical models: How far can we go with generative adversarial networks to reproduce stochastic processes? *Physica D: Nonlinear Phenomena*, 453:133831, 2023.
- [8] Niklas Wilming, Simon Harst, Nico Schmidt, and Peter König. Saccadic momentum and facilitation of return saccades contribute to an optimal foraging strategy. *PLoS computational biology*, 9(1):e1002871, 2013.

[9] Noa Malem-Shinitzki, Manfred Opper, Sebastian Reich, Lisa Schwetlick, Stefan A Seelig, and Ralf Engbert. A mathematical model of local and global attention in natural scene viewing. *PLoS Computational Biology*, 16(12):e1007880, 2020.

[10] Tim J Smith and John M Henderson. Facilitation of return during scene viewing. *Visual Cognition*, 17(6-7):1083–1108, 2009.

[11] Raymond M Klein and W Joseph MacInnes. Inhibition of return is a foraging facilitator in visual search. *Psychological science*, 10(4):346–352, 1999.

[12] Kelly Shen, Anthony R McIntosh, and Jennifer D Ryan. A working memory account of refixations in visual search. *Journal of vision*, 14(14):11–11, 2014.

[13] Matthias Kümmerer, Thomas SA Wallis, and Matthias Bethge. Information-theoretic model comparison unifies saliency metrics. *Proceedings of the National Academy of Sciences*, 112(52):16054–16059, 2015.

[14] Matthias Kümmerer, Matthias Bethge, and Thomas SA Wallis. Deepgaze iii: Modeling free-viewing human scanpaths with deep learning. *Journal of Vision*, 22(5):7–7, 2022.

[15] Henrik Thurfjell, Simone Ciuti, and Mark S Boyce. Applications of step-selection functions in ecology and conservation. *Movement ecology*, 2:1–12, 2014.

[16] Stefanie Muff, Johannes Signer, and John Fieberg. Accounting for individual-specific variation in habitat-selection studies: Efficient estimation of mixed-effects models using bayesian or frequentist computation. *Journal of Animal Ecology*, 89(1):80–92, 2020.

[17] Walter R Boot, Ensar Becic, and Arthur F Kramer. Stable individual differences in search strategy?: The effect of task demands and motivational factors on scanning strategy in visual search. *Journal of vision*, 9(3):7–7, 2009.

[18] Jennifer Wagner, Adriana Zurlo, and Elena Rusconi. Individual differences in visual search: A systematic review of the link between visual search performance and traits or abilities. *Cortex*, 2024.

[19] Timothy J Andrews and David M Coppola. Idiosyncratic characteristics of saccadic eye movements when viewing different visual environments. *Vision research*, 39(17):2947–2953, 1999.

[20] Keith Rayner, Xingshan Li, Carrick C Williams, Kyle R Cave, and Arnold D Well. Eye movements during information processing tasks: Individual differences and cultural effects. *Vision research*, 47(21):2714–2726, 2007.

[21] John M Henderson and Steven G Luke. Stable individual differences in saccadic eye movements during reading, pseudoreading, scene viewing, and scene search. *Journal of Experimental Psychology: Human Perception and Performance*, 40(4):1390, 2014.

[22] Ralf Engbert, Konstantin Mergenthaler, Petra Sinn, and Arkady Pikovsky. An integrated model of fixational eye movements and microsaccades. *Proceedings of the National Academy of Sciences*, 108(39):E765–E770, 2011.

[23] Christopher A Dickinson and Gregory J Zelinsky. Marking rejected distractors: A gaze-contingent technique for measuring memory during search. *Psychonomic Bulletin & Review*, 12(6):1120–1126, 2005.

[24] Tim J Smith and John M Henderson. Looking back at waldo: Oculomotor inhibition of return does not prevent return fixations. *Journal of Vision*, 11(1):3–3, 2011.

[25] Mengmi Zhang, Jiashi Feng, Keng Teck Ma, Joo Hwee Lim, Qi Zhao, and Gabriel Kreiman. Finding any waldo with zero-shot invariant and efficient visual search. *Nature communications*, 9(1):3730, 2018.

[26] Jeremy M Wolfe. Guided search 6.0: An updated model of visual search. *Psychonomic bulletin & review*, 28(4):1060–1092, 2021.

[27] Tilke Judd, Fredo Durand, and Antonio Torralba. Fixations on low-resolution images. *Journal of Vision*, 11(4):14–14, 2011.

[28] EAB Over, ITC Hooge, BNS Vlaskamp, and CJ17617434 Erkelens. Coarse-to-fine eye movement strategy in visual search. *Vision Research*, 47(17):2272–2280, 2007.

[29] Richard Cowan. Objects arranged randomly in space: an accessible theory. *Advances in Applied Probability*, 21(3):543–569, 1989.

[30] Benedikt V Ehinger, Lilli Kaufhold, and Peter König. Probing the temporal dynamics of the exploration–exploitation dilemma of eye movements. *Journal of vision*, 18(3):6–6, 2018.

[31] Bhavin R Sheth and Shinsuke Shimojo. Compression of space in visual memory. *Vision research*, 41(3):329–341, 2001.

[32] Iain D Gilchrist and Monika Harvey. Evidence for a systematic component within scan paths in visual search. *Visual cognition*, 14(4-8):704–715, 2006.

[33] Pieter JA Unema, Sebastian Pannasch, Markus Joos, and Boris M Velichkovsky. Time course of information processing during scene perception: The relationship between saccade amplitude and fixation duration. *Visual cognition*, 12(3):473–494, 2005.

[34] Heather Sheridan and Eyal M Reingold. The holistic processing account of visual expertise in medical image perception: A review. *Frontiers in psychology*, 8:1620, 2017.

[35] Evan F Risko, Nicola C Anderson, Sophie Lanthier, and Alan Kingstone. Curious eyes: Individual differences in personality predict eye movement behavior in scene-viewing. *Cognition*, 122(1):86–90, 2012.

[36] Colwyn B Trevarthen. Two mechanisms of vision in primates. *Psychologische Forschung*, 31(4):299–337, 1968.

[37] Christophe Lounis, Vsevolod Peysakhovich, and Mickaël Causse. Visual scanning strategies in the cockpit are modulated by pilots’ expertise: A flight simulator study. *PLoS one*, 16(2):e0247061, 2021.

[38] James D Forester, Hae Kyung Im, and Paul J Rathouz. Accounting for animal movement in estimation of resource selection functions: sampling and data analysis. *Ecology*, 90(12):3554–3565, 2009.

[39] Théo Michelot, Natasha J Klappstein, Jonathan R Potts, and John Fieberg. Understanding step selection analysis through numerical integration. *Methods in Ecology and Evolution*, 15(1):24–35, 2024.

[40] Eshin Jolly. Pymer4: Connecting r and python for linear mixed modeling. *Journal of Open Source Software*, 3(31):862, 2018.

Saccade crossing avoidance as a visual search strategy: Supplementary Information

Alex Szorkovszky* Rujeena Mathema, Pedro Lencastre, Pedro Lind, and Anis Yazidi

1 Eye tracking

Calibration was performed using a five point method. The EyeLink's internal classifier was used to classify saccades, fixations and blinks. The default threshold values were used for saccade detection ($30^{\circ}/s$ velocity, $8000^{\circ}/sec^2$ acceleration). The right eye positions and classifications were used for further analysis.

2 Preprocessing

After removing blinks and data points with abnormally high speed (over 40 pixels per ms, approximately 650 degrees per second) the x and y distributions of the Waldo task data were used to automatically correct miscalibrations. Using 100 bins in each direction, (allowing 15% on either side of the nominal screen boundaries) the final bin with a cumulative frequency under 0.5% and the first bin with a cumulative frequency over 99.5% were used as the data edges, and aligned to the screen dimensions by rescaling. Data points outside this region were then excluded. As a final cleaning stage, short segments below 20ms in length) were also discarded.

Participants with more than 20% of the 1000Hz data missing after preprocessing in either task were excluded (4 out of 35). The remaining participants had a mean of 1.1% missing fixations in the Waldo task and a mean of 1.0% missing fixations in the random pixel task (maximum 5.7% and 8.7% respectively). For remaining fixations, the landing times and the means of valid x and y positions were extracted.

3 Time constant optimization

Figure S1 shows the time constant optimization curves for both tasks. The peaks of the smoothed curves for the individual predictors were then used as the final time constants. This was done to preclude the possibility of further unmodeled history dependence that could affect a joint maximum.

When including the optima for the two other predictors, the curves peak at approximately the same height, and with only minor changes in shape.

3.1 Joint optimization

To further check for unseen dependencies between the chosen time-variable predictors, the DIRECT algorithm was used to determine the global optimum [1] as implemented in *SciPy 1.11.4*. A minimum proportional volume of 10^{-5} was used as a stopping criterion.

*Corresponding Author: alex@simula.no

4 Nonparametric model

This model is based on sampling from the empirical distribution

$$P(\Delta x_t, \Delta y_t | x_t, y_t) \quad (1)$$

where this is represented as a four dimensional histogram, normalized so that it sums to one for all pairs x_t, y_t . 50 bins were used in the x, y dimensions, and 100 in the Δ_x and Δ_y dimensions. Prior to normalization, gaussian kernel smoothing was applied. Two filter widths were used, $\sigma_{X,Y}$ for the x_t, y_t dimensions and $\sigma_{dX,dY}$ for the Δ_x and Δ_y dimensions, which were jointly optimized as detailed below.

4.1 Kernel smoothing optimization

For each combination of the smoothing parameters, a conditional distribution was obtained from the training data. A step selection process was then run on the test data, generating control points using the unconditional distribution $P(\Delta x_t, \Delta y_t)$ from the training data. The conditional probability in logits was then calculated from each smoothed conditional distribution for each case and control point. The log likelihood was then calculated by fitting the logistic regression model for each combination of $\sigma_{X,Y}$ and $\sigma_{dX,dY}$ in turn.

As shown in Figure S2, the optimal filter size is comparable to the screen dimensions, making the final distribution close to the unconditional one.

4.2 Amplitude spline

For the final fitting of the nonparametric model, the x and y displacements of sampled saccades were multiplied by a scaling factor $\exp(a_0 - a(t))$, where $a(t)$ was an estimate of the mean log saccade length over time t during a trial and a_0 was the overall mean log-length. The function $a(t)$ was obtained with a cubic spline fitted to an aggregated scatter plot of log-length against time in the trial, for all trials in the training data (see Figure S3). The *SciPy* function *splrev* was used to obtain the spline, with smoothing factor equal to the variance of log-length multiplied by the number of points. The mean and interquartile ranges of saccade log-lengths from the simulations, corresponding to Figure 3 in the main text, are also shown in Figure S3, along with the data and parametric models for comparison.

For the generative model, increments were first sampled based on the conditional distribution, then multiplied by the inverse of the scaling factor, i.e. $\exp(a(t) - a_0)$. Fixations outside the screen region were discarded and resampled.

5 Parametric model

5.1 Variable importance

The full parametric (logistic regression) models included the predictors in Figure 1 of the main text, as well as the linear saccade length, square of the log saccade length, initial distance from the center, all second-order interactions of these terms, plus the interaction between log-length and time to capture the coarse-to-fine transition.

To assess variable importance and linear effect sizes in the parametric model, we fit two models for each predictor: one with the predictor excluded, and one with only this predictor's interactions excluded. The AIC values obtained were each compared to that for the full model to determine the relative importance of linear terms and interactions. Z-scores were obtained for each model with the predictor's interactions removed. Figure S4 shows these z-scores and relative AIC contributions of each predictor, for both tasks.

5.2 Spatial dependence

To quantify the dependence on screen position, we used the change in sparsity ($\Delta s' = s' - s_0$) and change in distance from the centre ($\Delta c' = c' - c_0$) with a new candidate fixation, as well as the final sparsity s'

and initial distance from the centre c_0 . A logistic regression model was fit using these four terms and their interactions.

The gradients were then computed from the coefficients β as:

$$\frac{\partial L(c', s')}{\partial c'} \bigg|_{c'=c_0, s'=s_0} = \beta(c_0) + c\beta(c_0 : \Delta c) + s\beta(c_0 : \Delta s) \quad (2)$$

$$\frac{\partial L(c', s')}{\partial s'} \bigg|_{c'=c_0, s'=s_0} = \beta(\Delta s') + \beta(s') + c[\beta(c_0 : s') + \beta(c_0 : \Delta s)] + s\beta(\Delta s : s') \quad (3)$$

where $L(c, s)$ is the logit function and $:$ denotes interaction terms.

5.3 Self-crossings

Figure 3 of the main text contains saccade statistics that include both saccades for every self-crossing. When including only the first or only the second saccade in a crossing pair, the statistics are largely similar, as can be seen in Figure S5.

5.4 Stepwise regression

For the final parametric models (main text Figure 1 and Figure 3), all second-order interactions as well as $\log(r) * t$ were initially included, and stepwise backward elimination was used to exclude terms beginning with the highest p-value. A term's interaction with the log-length was not excluded if there was an existing interaction with the square of the log-length. The process is stopped at the first increase of the AIC. For the Waldo task, this reduced the final model from 120 to 83 terms. Using the same procedure on the random pixel task yielded 73 terms in the final model.

Outputs of the final model fits can be found at the end of this document in datasets 6.1 and 6.1.

6 Mixed-effect modelling

To limit the model's degrees of freedom, the mixed-effects logistic regression contained only linear fixed effects corresponding to the 12 predictors in Figure 1 of the main text, as well as the square of the log saccade distance. The training data was normalized to a mean of zero and a standard deviation of one for each predictors.

Figure S6 shows the significant individual differences for the random pixel task, equivalent to Figure 4 of the main text. Since the trial-level random effect was not fit, the intraclass correlation coefficient (ICC) was not estimated, and more significant predictors were also found for this reason.

Figure S7 shows the matrix of Pearson product-moment correlations between all pairs of random effects in both tasks.

For the Waldo task, the mean of the trial-median fixation duration was well correlated with the log saccade length, whether the latter was measured by the mean of the trial-median ($r = 0.53, p = 0.002$) or the random coefficient obtained from the logistic regression ($r = 0.55, p = 0.001$). These correlations can be seen in Figure S8.

6.1 Principal component analysis

PCA was run using the *PCA* class in *scikit-learn 1.2.2*. Since the variables were standardized, the resulting variances can be used as an estimate of each variable's importance. These were therefore not normalized again prior to principal component analysis. Figure S9 shows the loadings of the first three principal components for each task.

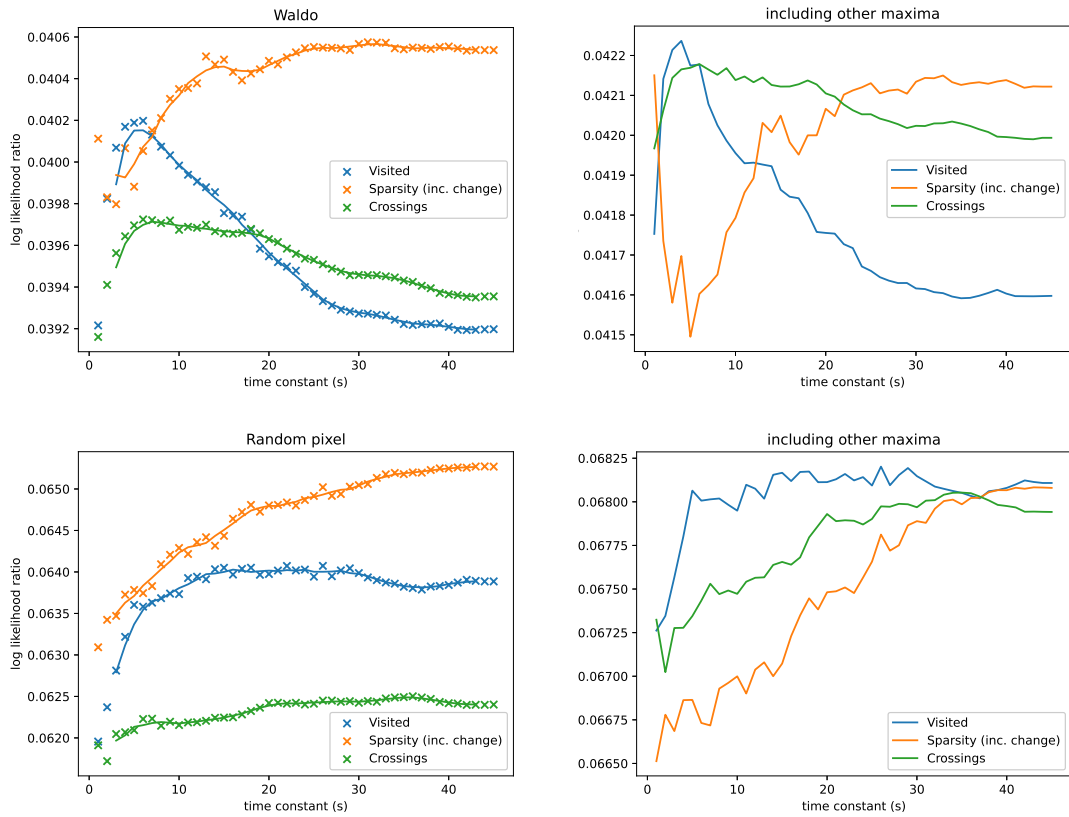


Fig. S1: Time constant optimization for the Waldo task (above) and the random pixel task (below). Left panels: Log-likelihood ratio vs τ for each of the three variable-history predictors when only one is included. The curve applies an average over a moving window of five seconds width. Right panels: The same time parameter sweeps, but including the maximum of the other two predictors.

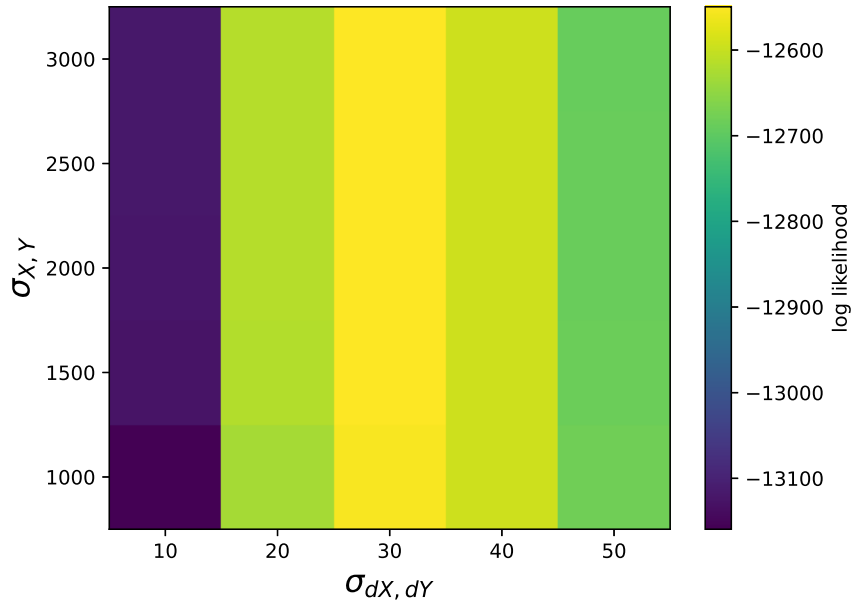


Fig. S2: Optimization of the KDE smoothing in the nonparametric model.

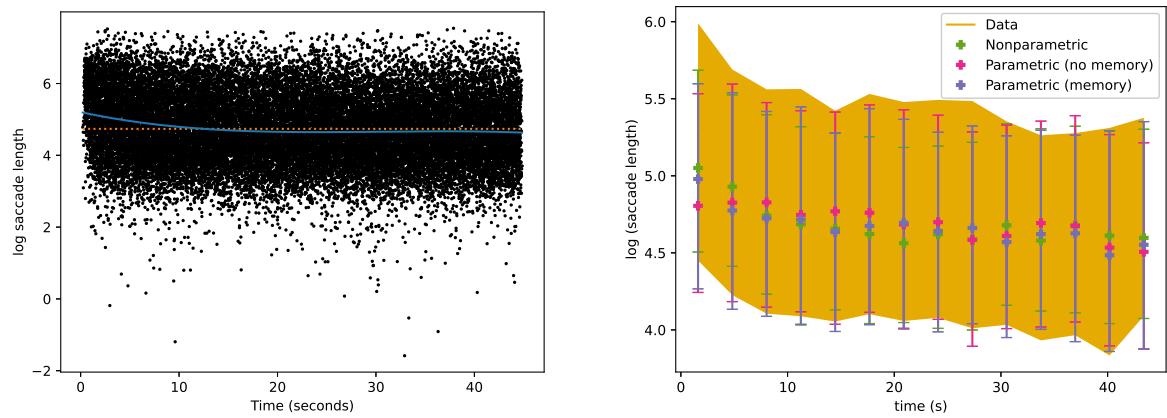


Fig. S3: Above: Fitting of the smoothing spline for the non-parametric model. Points are all saccade log-lengths in the training data. The solid line is the smoothing spline, and the dotted line is the overall mean. Below: Time evolution of mean log distance vs time for the data and the final models. Plotted are the median (line and points) and the interquartile range (region and errorbars).

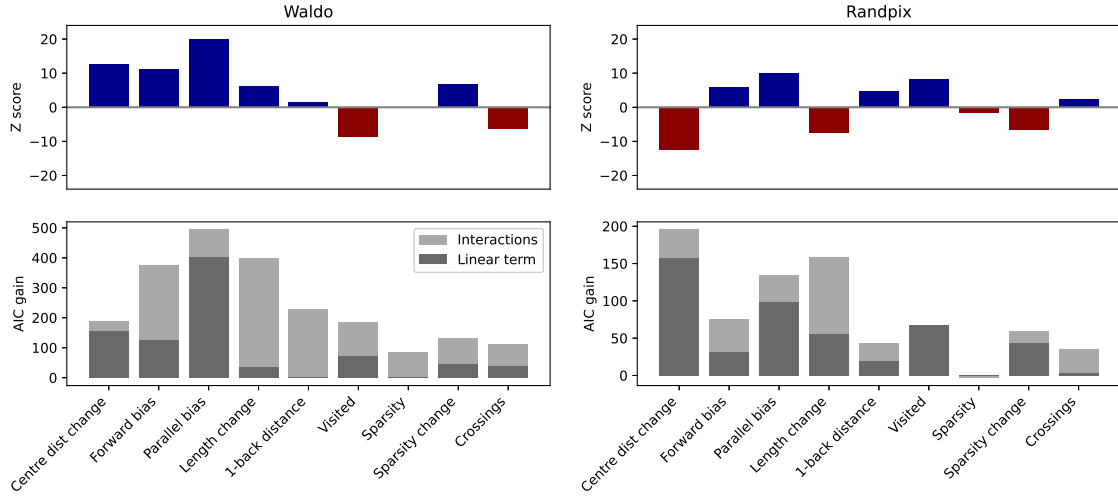


Fig. S4: Normalized effect sizes (z score) and AIC gains for each predictor. Z -scores were set to zero if the AIC gain for the linear model was negative.

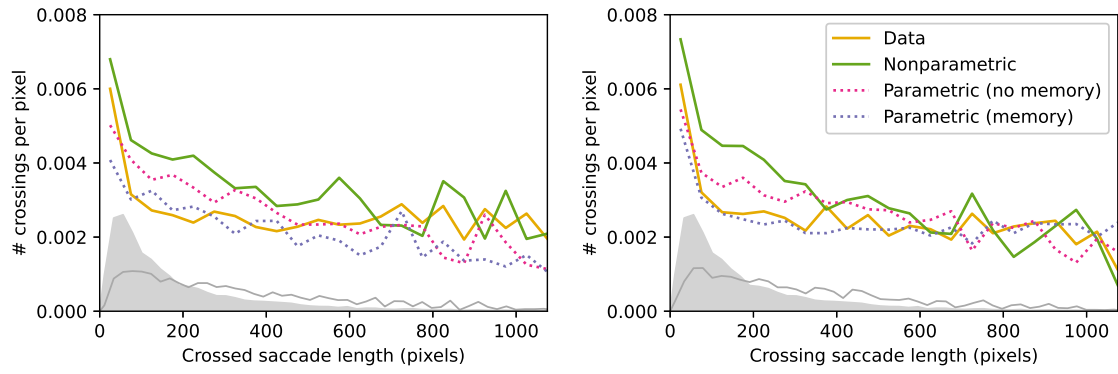


Fig. S5: Expected number of crossings per pixel for (left) the first saccade and (right) second saccade in a crossing pair, averaged over all saccades.

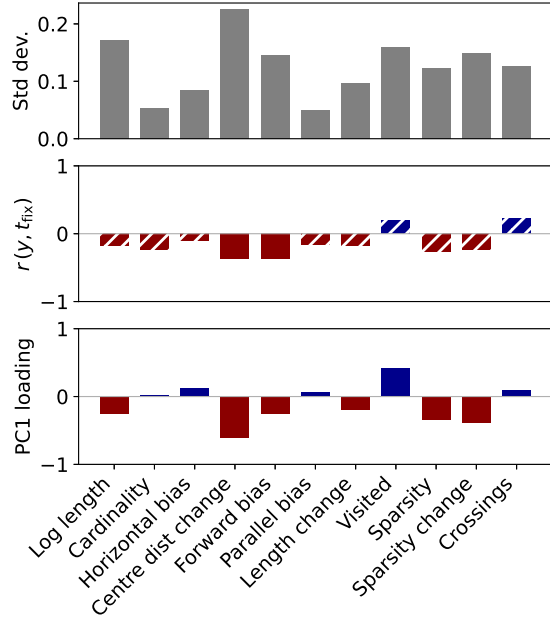


Fig. S6: Individual differences from the random pixel task. Top: Fitted standard deviation of random effects. Middle: Pearson product-moment correlations with means of the trial-level medians of fixation duration. Bottom: Loadings of the first principal component.

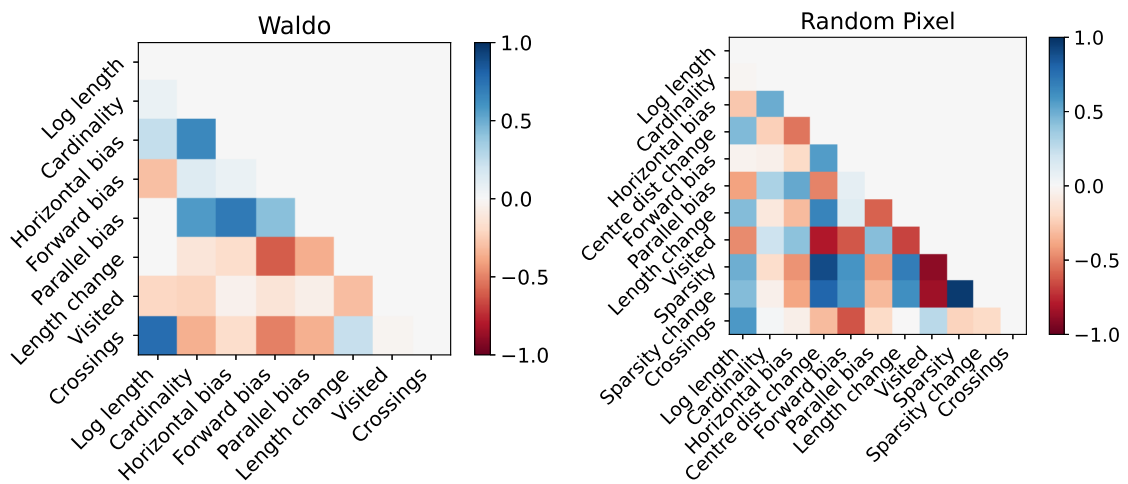


Fig. S7: Correlation matrices for fitted random effects for the significant predictors in each task. Note that the participant effect was not tested against a trial effect only model for the random pixel task.

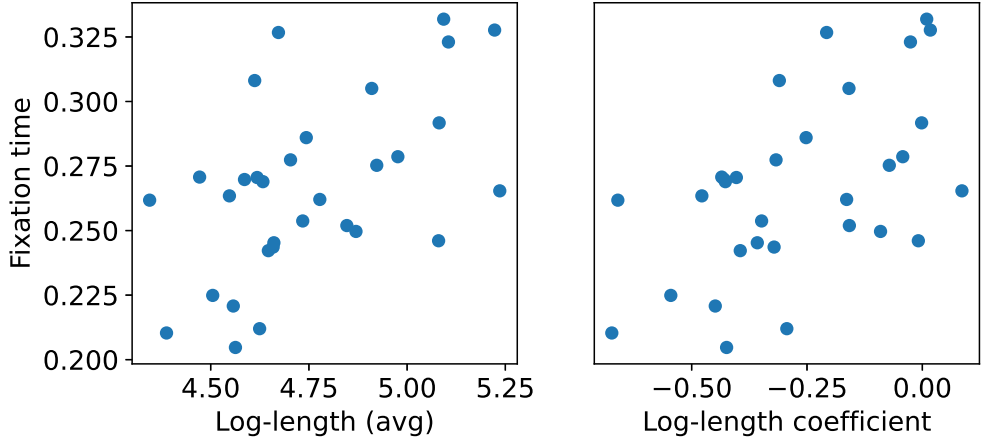


Fig. S8: Participant-level measures of fixation duration plotted against two participant-level measures of log saccade length for the Waldo task. The panel on the left uses a simple median of all saccade log-lengths per trial, with a mean then taken over the 9 trials. The panel on the right uses the random effect coefficients obtained for the *log length* predictor in the mixed-effect logistic regression. These are not centered at zero due to the addition of the fixed effect of *log length*.

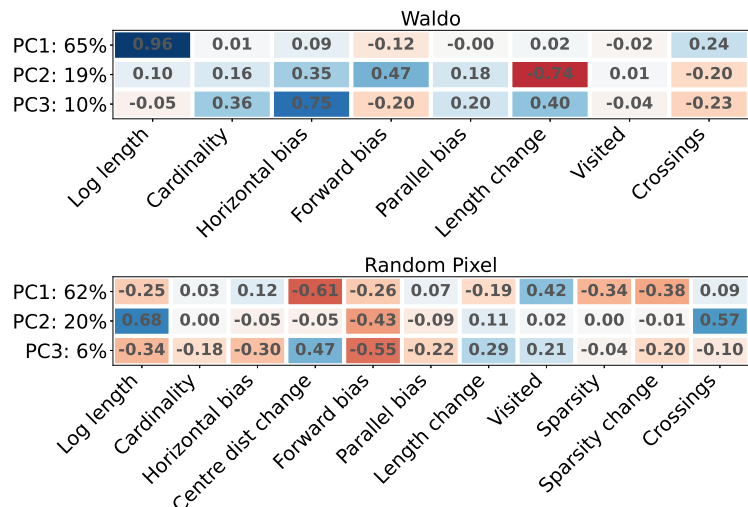


Fig. S9: Loadings of the first three principal components for each task. The variance explained is shown on the left of each row.

Dataset 1: Final logistic regression model for the Waldo task.

Glossary: `dir_change` is forward bias, `dir_change2` is parallel bias, and `whistdist` is sparsity.

Logit Regression Results						
Dep. Variable:	target	No. Observations:	280230			
Model:	Logit	Df Residuals:	280144			
Method:	MLE	Df Model:	85			
Date:	Fri, 22 Aug 2025	Pseudo R-squ.:	0.06520			
Time:	14:32:56	Log-Likelihood:	-85158.			
converged:	True	LL-Null:	-91098.			
Covariance Type:	nonrobust	LLR p-value:	0.000			
	coef	std err	z	P> z	[0.025	0.975]
Intercept	0.1015	1.338	0.076	0.940	-2.521	2.725
dist	-0.5503	0.055	-10.087	0.000	-0.657	-0.443
logdist	-1.0900	0.707	-1.542	0.123	-2.476	0.296
logdist_sq	0.6388	0.128	5.005	0.000	0.389	0.889
cardinality	0.4868	0.196	2.482	0.013	0.102	0.871
horiz_align	-0.2933	0.102	-2.866	0.004	-0.494	-0.093
centre_dist_change	0.0097	0.005	1.869	0.062	-0.000	0.020
dir_change	0.1724	0.195	0.883	0.377	-0.210	0.555
dir_change2	0.1599	0.192	0.834	0.404	-0.216	0.536
log_amp_change	-0.8505	0.106	-7.993	0.000	-1.059	-0.642
dist_1back	0.0001	0.002	0.070	0.944	-0.003	0.003
centre_dist_init	-0.0001	6.44e-05	-1.985	0.047	-0.000	-1.64e-06
have_visited	0.6755	0.107	6.342	0.000	0.467	0.884
whistdist	4.7592	2.366	2.011	0.044	0.122	9.397
whistdist_change	-20.5522	7.350	-2.796	0.005	-34.958	-6.146
crossings	2.0527	0.272	7.554	0.000	1.520	2.585
dist:logdist	0.1330	0.013	10.010	0.000	0.107	0.159
dist:logdist_sq	-0.0083	0.001	-9.779	0.000	-0.010	-0.007
dist:centre_dist_change	-3.886e-06	1.46e-06	-2.655	0.008	-6.75e-06	-1.02e-06
dist:log_amp_change	-0.0004	0.000	-3.315	0.001	-0.001	-0.000
dist:dist_1back	3.074e-06	8.63e-07	3.561	0.000	1.38e-06	4.77e-06
dist:centre_dist_init	2.497e-06	2.52e-07	9.906	0.000	2e-06	2.99e-06
dist:whistdist	-0.0082	0.002	-3.490	0.000	-0.013	-0.004
logdist:cardinality	-0.3379	0.078	-4.330	0.000	-0.491	-0.185
logdist:horiz_align	0.2057	0.014	14.632	0.000	0.178	0.233
logdist:centre_dist_change	-0.0043	0.002	-2.004	0.045	-0.009	-9.58e-05
logdist:dir_change	0.1781	0.083	2.138	0.033	0.015	0.341
logdist:dir_change2	0.1774	0.075	2.351	0.019	0.030	0.325
logdist:log_amp_change	0.2106	0.024	8.962	0.000	0.165	0.257
logdist:dist_1back	0.0010	0.001	1.420	0.156	-0.000	0.002
logdist:have_visited	-0.2036	0.024	-8.568	0.000	-0.250	-0.157
logdist:whistdist	-3.7318	1.220	-3.058	0.002	-6.124	-1.340
logdist:whistdist_change	8.1378	2.685	3.030	0.002	2.875	13.401
logdist:crossings	-0.8901	0.107	-8.284	0.000	-1.101	-0.679
logdist_sq:cardinality	0.0625	0.009	7.227	0.000	0.046	0.079
logdist_sq:centre_dist_change	0.0004	0.000	1.926	0.054	-7.82e-06	0.001
logdist_sq:dir_change	-0.0314	0.009	-3.424	0.001	-0.049	-0.013
logdist_sq:dir_change2	-0.0250	0.008	-3.009	0.003	-0.041	-0.009
logdist_sq:dist_1back	-0.0002	8.05e-05	-2.499	0.012	-0.000	-4.35e-05
logdist_sq:whistdist	0.6359	0.164	3.881	0.000	0.315	0.957
logdist_sq:whistdist_change	-0.6627	0.245	-2.701	0.007	-1.144	-0.182
logdist_sq:crossings	0.0925	0.011	8.344	0.000	0.071	0.114
cardinality:horiz_align	0.1537	0.020	7.845	0.000	0.115	0.192
cardinality:centre_dist_change	-0.0001	8.16e-05	-1.453	0.146	-0.000	4.13e-05
cardinality:dir_change	0.0730	0.014	5.038	0.000	0.045	0.101
cardinality:dir_change2	0.1092	0.014	7.577	0.000	0.081	0.137
cardinality:log_amp_change	0.0251	0.015	1.719	0.086	-0.004	0.054
cardinality:dist_1back	-0.0002	6.08e-05	-3.378	0.001	-0.000	-8.62e-05
cardinality:centre_dist_init	0.0002	4.07e-05	4.086	0.000	8.66e-05	0.000

cardinality:whistdist	-0.2307	0.144	-1.606	0.108	-0.512	0.051
cardinality:whistdist_change	-0.5130	0.224	-2.286	0.022	-0.953	-0.073
cardinality:crossings	-0.0352	0.016	-2.149	0.032	-0.067	-0.003
horiz_align:centre_dist_change	0.0003	9.96e-05	2.739	0.006	7.76e-05	0.000
horiz_align:dir_change	-0.0592	0.015	-3.979	0.000	-0.088	-0.030
horiz_align:dir_change2	-0.0206	0.014	-1.523	0.128	-0.047	0.006
horiz_align:log_amp_change	0.0449	0.014	3.161	0.002	0.017	0.073
horiz_align:dist_1back	-0.0002	6.91e-05	-2.291	0.022	-0.000	-2.29e-05
horiz_align:centre_dist_init	-0.0003	3.97e-05	-8.565	0.000	-0.000	-0.000
horiz_align:have_visited	0.0557	0.024	2.329	0.020	0.009	0.103
horiz_align:whistdist	-0.3750	0.143	-2.623	0.009	-0.655	-0.095
horiz_align:whistdist_change	0.3216	0.226	1.423	0.155	-0.121	0.765
horiz_align:crossings	-0.0336	0.016	-2.052	0.040	-0.066	-0.002
centre_dist_change:dir_change	-0.0001	7.41e-05	-1.563	0.118	-0.000	2.94e-05
centre_dist_change:log_amp_change	0.0002	5.5e-05	2.938	0.003	5.38e-05	0.000
centre_dist_change:dist_1back	4.785e-07	3.21e-07	1.490	0.136	-1.51e-07	1.11e-06
centre_dist_change:whistdist	0.0033	0.001	5.917	0.000	0.002	0.004
dir_change:log_amp_change	-0.2269	0.016	-14.064	0.000	-0.258	-0.195
dir_change:dist_1back	0.0008	6.6e-05	11.431	0.000	0.001	0.001
dir_change:have_visited	-0.1251	0.023	-5.412	0.000	-0.170	-0.080
dir_change2:log_amp_change	-0.0751	0.014	-5.219	0.000	-0.103	-0.047
dir_change2:dist_1back	0.0003	6.68e-05	4.799	0.000	0.000	0.000
dir_change2:centre_dist_init	-5.709e-05	3.89e-05	-1.466	0.143	-0.000	1.92e-05
dir_change2:whistdist	-0.3804	0.129	-2.950	0.003	-0.633	-0.128
dir_change2:crossings	0.0405	0.016	2.469	0.014	0.008	0.073
log_amp_change:dist_1back	-0.0004	7.45e-05	-5.288	0.000	-0.001	-0.000
log_amp_change:centre_dist_init	7.159e-05	3.66e-05	1.958	0.050	-7.56e-08	0.000
dist_1back:have_visited	0.0008	9.61e-05	7.893	0.000	0.001	0.001
dist_1back:crossings	-0.0002	6.76e-05	-2.686	0.007	-0.000	-4.9e-05
centre_dist_init:have_visited	-0.0002	6.24e-05	-3.254	0.001	-0.000	-8.07e-05
centre_dist_init:whistdist_change	0.0015	0.001	2.598	0.009	0.000	0.003
centre_dist_init:crossings	-8.964e-05	4.66e-05	-1.923	0.055	-0.000	1.74e-06
have_visited:whistdist_change	2.4732	0.444	5.569	0.000	1.603	3.344
have_visited:crossings	0.0507	0.027	1.897	0.058	-0.002	0.103
whistdist:whistdist_change	-6.0539	0.902	-6.709	0.000	-7.822	-4.285
t	0.0262	0.003	9.912	0.000	0.021	0.031
logdist:t	-0.0051	0.001	-9.073	0.000	-0.006	-0.004
=====						

Dataset 2: Final logistic regression model for the random pixel task

Logit Regression Results						
Dep. Variable:	target	No. Observations:	59990			
Model:	Logit	Df Residuals:	59914			
Method:	MLE	Df Model:	75			
Date:	Fri, 22 Aug 2025	Pseudo R-squ.:	0.1047			
Time:	15:31:37	Log-Likelihood:	-17459.			
converged:	True	LL-Null:	-19502.			
Covariance Type:	nonrobust	LLR p-value:	0.000			
		coef	std err	z	P> z	[0.025 0.975]
Intercept		5.9969	3.173	1.890	0.059	-0.223 12.217
dist		-0.3804	0.143	-2.651	0.008	-0.662 -0.099
logdist		-3.7599	1.645	-2.286	0.022	-6.984 -0.536
logdist_sq		0.8046	0.330	2.437	0.015	0.157 1.452
cardinality		0.0831	0.043	1.938	0.053	-0.001 0.167
horiz_align		-1.4787	0.833	-1.775	0.076	-3.111 0.154
centre_dist_change		0.0426	0.014	3.119	0.002	0.016 0.069
dir_change		-0.4068	0.254	-1.602	0.109	-0.905 0.091
dir_change2		-0.4615	0.524	-0.881	0.378	-1.488 0.565
log_amp_change		-2.2676	0.277	-8.191	0.000	-2.810 -1.725
dist_1back		0.0057	0.002	2.879	0.004	0.002 0.010
centre_dist_init		0.0007	0.001	0.940	0.347	-0.001 0.002
have_visited		-0.6950	0.422	-1.649	0.099	-1.521 0.131
whistdist		16.3161	5.799	2.813	0.005	4.950 27.683
whistdist_change		26.4451	11.556	2.288	0.022	3.796 49.095
crossings		0.8607	0.234	3.673	0.000	0.401 1.320
dist:logdist		0.0933	0.034	2.742	0.006	0.027 0.160
dist:logdist_sq		-0.0060	0.002	-2.826	0.005	-0.010 -0.002
dist:cardinality		0.0009	0.000	7.351	0.000	0.001 0.001
dist:horiz_align		0.0019	0.001	2.637	0.008	0.000 0.003
dist:centre_dist_change		-1.431e-05	3.51e-06	-4.074	0.000	-2.12e-05 -7.42e-06
dist:dir_change		-0.0007	0.000	-2.183	0.029	-0.001 -7.36e-05
dist:log_amp_change		-0.0004	0.000	-1.738	0.082	-0.001 5.69e-05
dist:dist_1back		1.81e-06	1.1e-06	1.648	0.099	-3.43e-07 3.96e-06
dist:centre_dist_init		3.863e-06	1.13e-06	3.420	0.001	1.65e-06 6.08e-06
dist:have_visited		-0.0011	0.000	-2.803	0.005	-0.002 -0.000
dist:whistdist		-0.0125	0.005	-2.622	0.009	-0.022 -0.003
logdist:horiz_align		0.8875	0.417	2.128	0.033	0.070 1.705
logdist:centre_dist_change		-0.0196	0.006	-3.516	0.000	-0.030 -0.009
logdist:dir_change		0.1366	0.059	2.322	0.020	0.021 0.252
logdist:dir_change2		0.4967	0.212	2.339	0.019	0.080 0.913
logdist:log_amp_change		0.4328	0.061	7.151	0.000	0.314 0.551
logdist:dist_1back		-0.0011	0.000	-2.910	0.004	-0.002 -0.000
logdist:centre_dist_init		-0.0004	0.000	-2.251	0.024	-0.001 -5.25e-05
logdist:have_visited		0.1672	0.087	1.928	0.054	-0.003 0.337
logdist:whistdist		-8.5962	2.839	-3.027	0.002	-14.161 -3.031
logdist:whistdist_change		-10.1921	4.301	-2.370	0.018	-18.622 -1.763
logdist:crossings		-0.2944	0.086	-3.413	0.001	-0.463 -0.125
logdist_sq:horiz_align		-0.1064	0.055	-1.952	0.051	-0.213 0.000
logdist_sq:centre_dist_change		0.0022	0.001	3.702	0.000	0.001 0.003
logdist_sq:dir_change2		-0.0673	0.022	-3.028	0.002	-0.111 -0.024
logdist_sq:whistdist		1.1161	0.365	3.057	0.002	0.400 1.832
logdist_sq:whistdist_change		0.8828	0.401	2.199	0.028	0.096 1.670
logdist_sq:crossings		0.0286	0.008	3.545	0.000	0.013 0.044
cardinality:horiz_align		0.1053	0.043	2.468	0.014	0.022 0.189
cardinality:log_amp_change		-0.0452	0.030	-1.524	0.127	-0.103 0.013
horiz_align:centre_dist_change		0.0004	0.000	2.171	0.030	3.75e-05 0.001
horiz_align:dir_change		-0.0727	0.035	-2.094	0.036	-0.141 -0.005
horiz_align:dist_1back		-0.0004	0.000	-2.955	0.003	-0.001 -0.000

horiz_align:centre_dist_init	-0.0004	9.31e-05	-3.969	0.000	-0.001	-0.000
horiz_align:whistdist_change	1.3570	0.335	4.056	0.000	0.701	2.013
centre_dist_change:dir_change	0.0003	0.000	1.907	0.057	-8.57e-06	0.001
centre_dist_change:dir_change2	-0.0002	0.000	-1.565	0.118	-0.000	4.9e-05
centre_dist_change:dist_1back	8.017e-07	5.54e-07	1.446	0.148	-2.85e-07	1.89e-06
centre_dist_change:centre_dist_init	1.554e-06	4.06e-07	3.830	0.000	7.59e-07	2.35e-06
centre_dist_change:whistdist_change	-0.0016	0.001	-1.562	0.118	-0.004	0.000
dir_change:log_amp_change	-0.1949	0.041	-4.752	0.000	-0.275	-0.115
dir_change:dist_1back	0.0006	0.000	4.029	0.000	0.000	0.001
dir_change:centre_dist_init	0.0004	0.000	3.449	0.001	0.000	0.001
dir_change:whistdist_change	-0.5960	0.270	-2.209	0.027	-1.125	-0.067
dir_change2:log_amp_change	-0.1558	0.034	-4.596	0.000	-0.222	-0.089
dir_change2:dist_1back	0.0004	0.000	3.146	0.002	0.000	0.001
dir_change2:have_visited	-0.0724	0.048	-1.508	0.132	-0.166	0.022
dir_change2:whistdist_change	-0.5701	0.304	-1.878	0.060	-1.165	0.025
dir_change2:crossings	0.0152	0.008	1.990	0.047	0.000	0.030
log_amp_change:dist_1back	-0.0004	0.000	-2.439	0.015	-0.001	-8.69e-05
dist_1back:centre_dist_init	1.232e-06	3.61e-07	3.416	0.001	5.25e-07	1.94e-06
centre_dist_init:whistdist_change	-0.0023	0.001	-1.807	0.071	-0.005	0.000
centre_dist_init:crossings	-6.674e-05	2.96e-05	-2.255	0.024	-0.000	-8.73e-06
have_visited:whistdist	0.7664	0.400	1.914	0.056	-0.018	1.551
have_visited:crossings	0.0258	0.014	1.871	0.061	-0.001	0.053
whistdist:whistdist_change	2.3364	1.313	1.779	0.075	-0.238	4.910
whistdist:crossings	-0.2686	0.078	-3.434	0.001	-0.422	-0.115
whistdist_change:crossings	-0.1513	0.085	-1.781	0.075	-0.318	0.015
t	0.0408	0.007	5.488	0.000	0.026	0.055
logdist:t	-0.0089	0.001	-6.103	0.000	-0.012	-0.006

References

[1] Donald R Jones, Cary D Perttunen, and Bruce E Stuckman. Lipschitzian optimization without the lipschitz constant. *Journal of optimization Theory and Applications*, 79(1):157–181, 1993.